INTERNATIONAL CONFERENCE FLUID POWER 2021
CONFERENCE PROCEEDINGS
D. Lovrec & V. Tič (eds.)

University of Maribor Press

Challenges of numerical modelling and simulation of flow inside the hydraulic tank

LUKA KEVORKIJAN & IGNACIJO BILUŠ

Abstract The basic purpose of the hydraulic tank is to hold a volume of fluid, transfer heat from the system, allow solid contaminants to settle and facilitate the release of air and moisture from the fluid. To perform these important tasks more efficiently, the tank must be properly dimensioned and it must operate in correct flow rate range. At high flow rates it can be subjected to effects of turbulence, leading to poorer performance of the tank. To predict turbulent effects correctly a numerical simulation, based on RANS approach is prepared and run. Difference between $k-\varepsilon$ model and $k-\omega$ Shear Stress Transport (SST) is investigated and results are presented. Impact of choice of turbulence model is discussed.

Keywords: • hydraulic tank • turbulence modelling • wall y^+ • RANS • simulation •

CORRESPONDENCE ADDRESS: Luka Kevorkijan, University of Maribor, Faculty of Mechanical Engineering, Smetanova 17, 2000 Maribor, Slovenia, e-mail: luka.kevorkijan@um.si. Ignacijo Biluš, University of Maribor, Faculty of Mechanical Engineering, Smetanova 17, 2000 Maribor, Slovenia, e-mail: ignacijo.bilus@um.si.

DOI https://doi.org/10.18690/978-961-286-513-9.12 ISBN 978-961-286-513-9
Dostopno na: http://press.um.si

1 Introduction

One of the functions of a hydraulic tank is to remove air bubbles and particulate contaminants that have been introduced into hydraulic fluid due to various reasons, among them leaks in the pipe connections and wear of hydraulic system components. Depending on flow conditions (turbulent intensity) particles settle and air bubbles rise with varying degree of efficiency, less disturbed and turbulent flow allows for a higher efficiency of removal of contaminants.

In anticipation of occurrence of unfavourable flow conditions it can be beneficial to have detailed information about the flow inside the hydraulic tank before the final design is decided. For this purpose a computational fluid dynamics (CFD) study can be performed on an early design proposal (or to analyse existing tank). However, as complexity of analysed flow increases so does the complexity of modelling the flow.

With respect to flow rate (or velocity) through the tank, two distinct types of flow occur, laminar and turbulent. Turbulent flow introduces additional complexity in description of the flow and different approaches exist to obtain numerical solution of turbulent flow. From practical standpoint RANS approach provides a good balance between computational effort, modelling complexity and accuracy of predicting turbulence in the flow. Within the RANS approach different models based on Boussinesq hypothesis exist. These are classified by number of additional equations to model turbulent viscosity, such as one equation Spalart-Allmaras model and several two equation models among them k-epsilon (k-ε), k-omega (k-ω) and Menter's Shear Stress Transport (SST) model [1], [2].

In this work we applied the k-epsilon (k-ε) model and Menter's Shear Stress Transport (SST) model and compared the resulting flow.

2 Numerical modelling

An Eulerian approach to describe fluid flow is used in this study. This approach is implemented and readily available in commercial CFD solvers, in this study ANSYS CFX 2020 R2 was used [2]. In all simulations the flow was isothermal with fluid properties listed in Table 1 and steady-state mode was selected.

Table 1: Liquid properties used in simulations

Liquid (Oil)	Density [kg/m³]	Dynamic viscosity [kg/m s]	Kinematic viscosity [m²/s]
ISO VG 22	856.8	0.018147024	0.00002118

Fluid flow is described with continuity equation:

$$\frac{\partial \rho}{\partial t} + \vec{\nabla} \cdot (\rho \vec{u}) = 0 \tag{1}$$

and Navier-Stokes equations:

$$\frac{\partial (\rho \vec{u})}{\partial t} + \rho(\vec{u} \cdot \vec{\nabla})\vec{u} = -\vec{\nabla} p + \mu \nabla^2 \vec{u} + \rho \vec{g} \tag{2}$$

where ρ is fluid density, $\vec{u}$ is fluid velocity, p is pressure, μ is fluid dynamic viscosity and $\vec{g}$ is gravitational acceleration.

To model turbulent flow equations (1) and (2) are Reynolds-averaged and the resulting equations are Reynolds-Averaged Navier-Stokes equations (RANS). Any time dependent flow variable $\phi(t)$ is split:

$$\phi(t) = \overline{\phi}(t) + \phi'(t) \tag{3}$$

So that $\overline{\phi}(t)$ represents a mean value and $\phi'(t)$ represents time-dependent fluctuation with respect to this mean value. Mean value is obtained by applying sliding time-averaging window:

$$\overline{\phi}(t) = \frac{1}{2\Delta t} \int_{t-\Delta t}^{t+\Delta t} \phi(t) dt \tag{4}$$

where the time-averaging window is written as an interval $[t - \Delta t, t + \Delta t\,]$.

After applying the Reynolds averaging procedure, continuity equation is rewritten as:

$$\frac{\partial \rho}{\partial t} + \vec{\nabla} \cdot \left(\rho \overline{\vec{u}}\right) = 0 \tag{5}$$

And Navier-Stokes equations (RANS) are rewritten as:

$$\frac{\partial \left(\rho \overline{\vec{u}}\right)}{\partial t} + \rho \left(\overline{\vec{u}} \cdot \vec{\nabla}\right) \overline{\vec{u}} = -\vec{\nabla} \overline{p} + \mu \nabla^2 \overline{\vec{u}} - \vec{\nabla} \cdot \left(\rho \overline{\vec{u'} \vec{u'}}\right) + \rho \vec{g} \tag{6}$$

where $\overline{\vec{u}}$ is now a mean flow velocity, $\overline{p}$ a mean pressure and $\overline{\vec{u'}}$ is fluctuation of fluid flow velocity with respect to its mean value. An additional term in equation (6) arises as a result of averaging procedure, named Reynolds stress. In this work this term is modelled based on the Boussinesq hypothesis:

$$\rho \overline{\vec{u'} \vec{u'}} = \mu_t \left[\left(\vec{\nabla} \overline{\vec{u}} + \vec{\nabla} \overline{\vec{u}}^T\right) - \frac{2}{3} \left(\vec{\nabla} \cdot \overline{\vec{u}}\right) \overline{\vec{I}}\right] \tag{7}$$

where a turbulent viscosity μ_t is introduced and $\overline{\vec{I}}$ is the identity matrix.

Turbulent viscosity is expressed with turbulent kinetic (k) energy and rate of dissipation of turbulent kinetic energy (ε) within the $k - \varepsilon$ turbulent model formulation:

$$\mu_t = C_\mu \rho \frac{k^2}{\varepsilon} \tag{8}$$

To model turbulent viscosity two additional transport equations for two turbulent variables are introduced. Turbulent kinetic energy is defined as:

$$k = \frac{1}{2} \left(\overline{u_x{}' u_x{}'} + \overline{u_y{}' u_y{}'} + \overline{u_z{}' u_z{}'}\right) \tag{9}$$

For two equation turbulence models isotropy of turbulence is assumed $\overline{u_x{}' u_x{}'} = \overline{u_y{}' u_y{}'} = \overline{u_z{}' u_z{}'}$ and transport equation for turbulent kinetic energy is written

$$\frac{\partial (\rho k)}{\partial t} + \vec{\nabla} \cdot (\rho k \overline{\vec{u}}) = \vec{\nabla} \cdot \left[\left(\mu + \frac{\mu_t}{\sigma_k}\right) \vec{\nabla} k\right] + P_k - \rho \varepsilon \tag{10}$$

For *k-ε* model the second transport equation is written for transport of the rate of dissipation of turbulent kinetic energy (ε)

$$\frac{\partial(\rho\varepsilon)}{\partial t} + \vec{\nabla}\cdot(\rho\varepsilon\vec{\boldsymbol{u}}) = \vec{\nabla}\cdot\left[\left(\mu + \frac{\mu_t}{\sigma_\varepsilon}\right)\vec{\nabla}\varepsilon\right] + \frac{\varepsilon}{k}(C_{\varepsilon 1}P_k - C_{\varepsilon 2}\rho\varepsilon) \qquad (11)$$

In equations (8) and (9) P_k is production of turbulent kinetic energy, additional terms are sometimes added to account for buoyancy and other effects. Model parameters are listed in Table 2.

Table 2: *k-ε* turbulent model parameters

$C_{\varepsilon 1}$	$C_{\varepsilon 2}$	σ_k	σ_ε	σ_μ
1.44	1.92	1.0	1.3	0.09

Another two equation turbulence model is *k-ω* Shear Stress Transport (SST) model. Turbulent viscosity is then expressed as:

$$\mu_t = \frac{\rho k}{\omega}\frac{1}{max\left[\frac{1}{\alpha^*}, \frac{SF_2}{a_1\omega}\right]} \qquad (12)$$

where $\omega = \varepsilon/k$ is specific rate of dissipation of turbulent kinetic energy, $\alpha^*$is low Reynolds number damping coefficient set to 1 in a high Reynolds number flow, a_1 is a model constant, S is the strain rate magnitude and F_2 is the second blending function. Strain rate magnitude is defined as:

$$S = \sqrt{2\overline{\overline{\boldsymbol{S}}}\,\overline{\overline{\boldsymbol{S}}}} \qquad (13)$$

where $\overline{\overline{\boldsymbol{S}}}$ is the strain rate tensor:

$$\overline{\overline{\boldsymbol{S}}} = \frac{1}{2}\left(\vec{\nabla}\vec{\boldsymbol{u}} + \vec{\nabla}\vec{\boldsymbol{u}}^T\right) \qquad (14)$$

Second blending function is defined as

$$F_2 = tanh\left[\left[max\left(\frac{2\sqrt{k}}{\beta^*\omega y}, \frac{500\nu}{y^2\omega}\right)\right]^2\right] \qquad (15)$$

where β^* is a model constant, y is distance to the wall and ν is kinematic viscosity of fluid. Transport equations for turbulent kinetic energy (k) and for specific rate of dissipation of turbulent kinetic energy (ω) are:

$$\frac{\partial(\rho k)}{\partial t} + \vec{\nabla} \cdot (\rho k \vec{\boldsymbol{u}}) = \vec{\nabla} \cdot \left[\left(\mu + \frac{\mu_t}{\sigma_k}\right)\vec{\nabla} k\right] + P_k - \rho\beta^* k\omega \tag{16}$$

$$\frac{\partial(\rho\omega)}{\partial t} + \vec{\nabla} \cdot (\rho\omega \vec{\boldsymbol{u}}) = \vec{\nabla} \cdot \left[\left(\mu + \frac{\mu_t}{\sigma_\omega}\right)\vec{\nabla}\omega\right] + \rho\frac{\gamma}{\mu_t} - \beta\rho\omega^2 + 2(1 - F_1)\frac{\rho\sigma_{\omega,2}}{\omega}\left(\vec{\nabla} k\right) \cdot \left(\vec{\nabla}\omega\right) \tag{17}$$

where P_k is production of turbulent kinetic energy, β is a model parameter, F_1 is the first blending function and $\sigma_{\omega,2}$ is a model constant. σ_k, σ_ω are model parameters further defined as:

$$\sigma_k = \frac{1}{F_1/\sigma_{k,1} + (1 - F_2)/\sigma_{k,2}} \tag{18}$$

$$\sigma_\omega = \frac{1}{F_1/\sigma_{\omega,1} + (1 - F_2)/\sigma_{\omega,2}} \tag{19}$$

where $\sigma_{k,1}$, $\sigma_{k,2}$ and $\sigma_{\omega,1}$ are model constants.

The first blending function is defined as:

$$F_1 = tanh\left[\left[min\left[max\left(\frac{\sqrt{k}}{\beta^*\omega y}, \frac{500\nu}{y^2\omega}\right), \frac{4\sigma_{\omega 2} k}{CD_{k\omega} y^2}\right]\right]^4\right] \tag{20}$$

where $CD_{k\omega}$ is defined as

$$CD_{k\omega} = max\left(2\rho\sigma_{\omega 2}\frac{1}{\omega}\left(\vec{\nabla} k\right) \cdot \left(\vec{\nabla}\omega\right), 10^{-10}\right) \tag{21}$$

Model constants are listed in Table 3.

Table 3: *k-w* Shear Stress Transport (SST) model constants

α^*	a_1	β^*	$\sigma_{k,1}$	$\sigma_{k,2}$	$\sigma_{\omega,1}$	$\sigma_{\omega,2}$
1	0.31	0.09	1.176	1.0	2.0	1.168

3 Geometry and computational mesh

In this study the analysed geometry was a hydraulic tank WN-LC-63-1RO with 30 litre capacity, shown in Figure 1.

Two turbulent models under consideration have different requirements for near wall mesh cell size (density). With standard *k-ω* model a standard log-law wall function approach is employed, therefore the recommended dimensionless wall distance is: [2], [3]

$$30 < y^+ < 300 \tag{22}$$

Dimensionless wall distance (y^+) is defined as:

$$y^+ = \frac{y}{\nu}\sqrt{\frac{\tau_w}{\rho}} \tag{23}$$

where y is normal distance from cell centroid to the nearest wall, ν is the kinematic viscosity of fluid, τ_w is the wall shear stress and ρ is fluid density.

For *k-ω* SST the condition for y^+ is more relaxed, however the benefit of this turbulent model is for sufficiently small values of $y^+ < 5$ (sufficient mesh density near the wall) viscous sublayer can be resolved [2], [3]. This is beneficial for situations with adverse pressure gradients and separation of flow, where standard *k-ε* fails to correctly predict the flow.

Because of different required mesh densities near the wall, two meshes were created, one for each turbulent model. Details about both meshes are presented in Table 4 and difference in mesh density near the wall is visible in Figure 2.

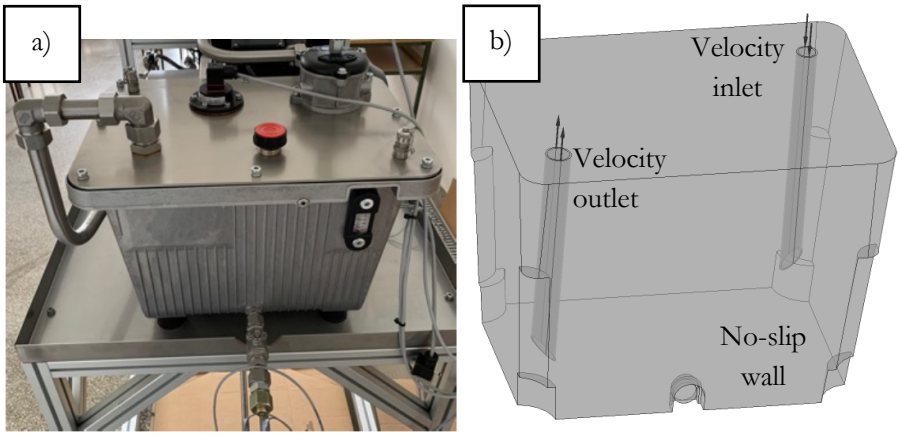

Figure 1: Considered hydraulic tank
a) appearance of the tank [3], b) computer generated 3D geometric model.

Table 4: Mesh metrics

Mesh name	Number of elements	Minimum element orthogonality	Maximum element aspect ratio	Minimum value of y^+	Maximum value of y^+
M1	366 862	0.0533	22.96	0	54.86
M2	2 675 435	0.0499	6708	0	0.4312

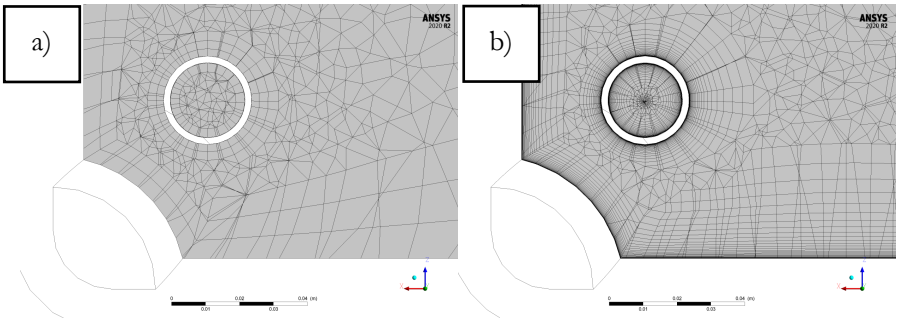

Figure 2: Geometry cut with a plane parallel to the bottom of the tank, visible corner with cut intake pipe;
a) mesh M1, b) mesh M2.

4 Boundary conditions and simulation setup

To ensure that turbulent flow is present inside the tank, flow rate through the tank was set such, that high enough Reynolds number in both the intake pipe and outtake pipe was achieved, as seen in Table 5. Both inlet and outlet boundary condition were prescribed as average inlet and outlet velocity, all other surfaces of the tank were taken as no-slip walls, as shown on Figure 2 b).

Table 5: Intake and outtake boundary conditions

Flow Rate [l/min]	Re_{intake}	$Re_{outtake}$	Average intake velocity [m/s]	Average outtake velocity [m/s]
60	2755	2164	2.675	1.651

Reference pressure within computational domain was set to 1 atm, turbulence intensity was set to 1 % as initial condition and as inlet boundary condition. Both advection and turbulent numeric scheme was chosen to be high resolution and Root Mean Square (RMS) convergence criterion was set to 10^{-4} for all equations. For velocity-pressure coupling Fourth Order Rhie Chow option was selected.

5 Results and conclusions

Both turbulent models resulted in flow with similar main features, such as vortices in the centre of the tank and close to the outtake pipe. This is shown visible in Figure 3 and Figure 4, where streamlines and velocity vector field are shown.

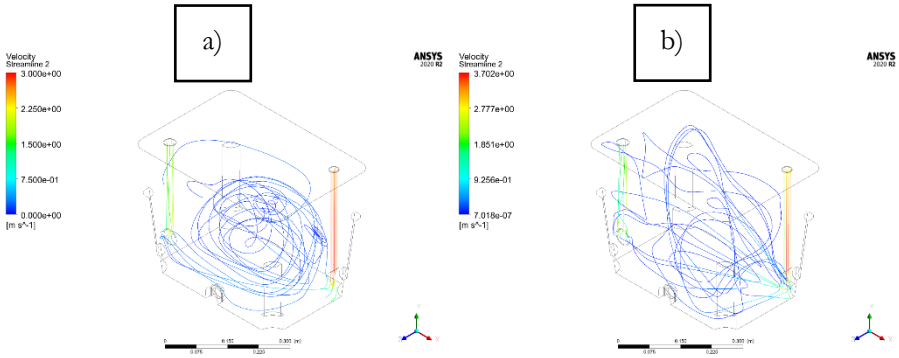

Figure 3: Streamlines, coloured by fluid velocity; a) k-ε model, b) k-ω SST model

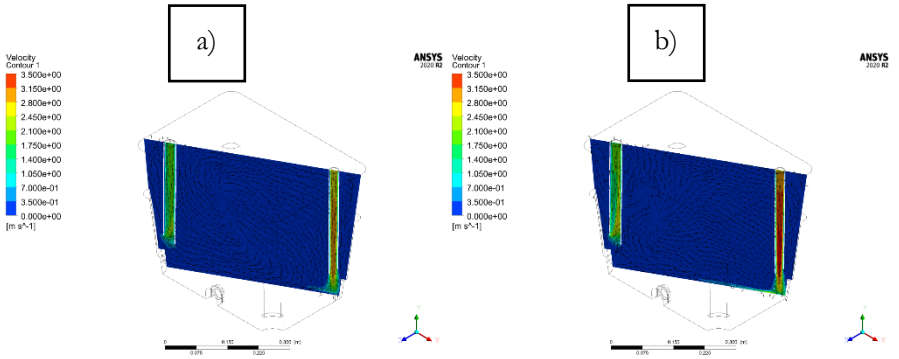

Figure 4: Velocity contour with normalized velocity vector field; a) k-ε model, b) k-ω SST model.

Significant differences are seen in comparison of predicted wall shear strain rate, shown in Figure 5. Both models predict the highest values of shear strain rate on the bottom wall in the corner underneath the oil tank intake pipe, however $k-\varepsilon$ model predicts lower values compared to k-ω SST model. Although general features of the fluid flow were recognized to be similar for both turbulent models, a more detailed presentation is shown in Figure 6, where velocity magnitude is plotted along the height of the tank in the centre of the tank. From these velocity profiles it is apparent that k-ω SST model predicts different velocity profile compared to k-ε model, particularly higher velocity gradient on the bottom and top wall is observed in the case of k-ω SST model.

It should be noted that the difference in velocity profile could arise as a consequence of vastly different mesh densities in the bulk of the flow as well as near the wall, resulting in corresponding difference in flow solution resolution.

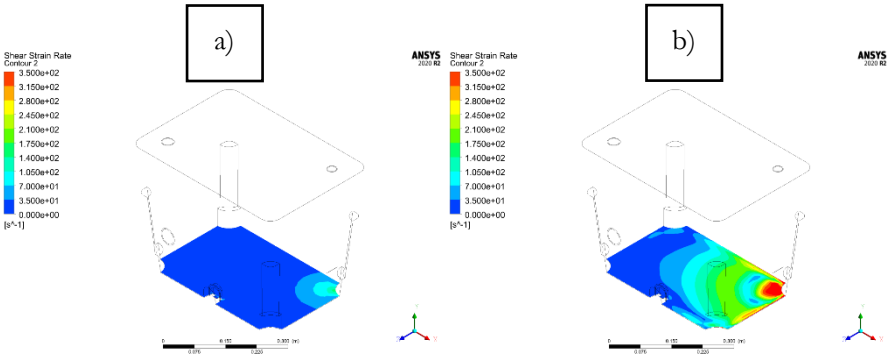

Figure 5: Shear strain rate on the bottom wall of the tank; a) *k-ε* model, b) *k-ω* SST model.

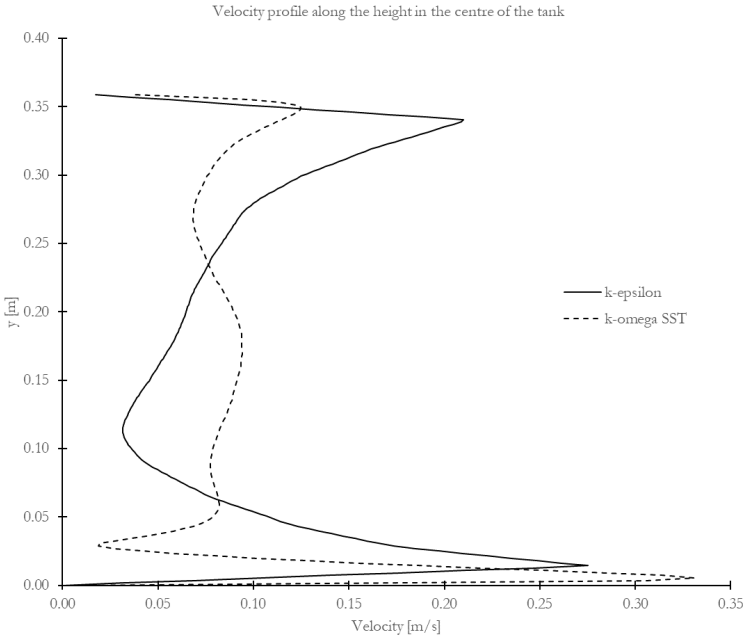

Figure 9: Vertical velocity profiles in the centre of the tank for both turbulent models under consideration.

6 Discussion

Both turbulence models gave similar flow field prediction. In the case of k-ω SST model higher shear strain rates were calculated, which would indicate more intensive energy dissipation. It would follow then that due to higher flow disturbance bubbles and particles would take longer to rise or to settle.

To validate the results and determine, which model is more appropriate comparison to experiment should be made. An interesting research avenue would be also to include thermal effects on predicted flow, particularly in combination with temperature dependent oil viscosity.

At the end it should be noted that for different flow rates or oil viscosity, the flow regime could become laminar, rendering turbulence modelling unnecessary.

References

[1] Škerget, L. (1994). Mehanika tekočin. Tehniška fakulteta v Mariboru, Univerza v Mariboru in Fakulteta za strojništvo v Ljubljani, Univerza v Ljubljani.

[2] ANSYS CFX Solver-Theory Guide (2020). ANSYS, Inc., 275 Technology Drive Canonsburg,PA 15317.

[3] Cesar, J. (2020). Numerical Analysis of Flow in the Small Hydraulic Tank WN-LC-63-1RO. Bachelor thesis, Faculty of Mechanical Engineering, University of Maribor.

[4] Lovrec, D. (2018). Fizikalno ozadje delovanja hidravličnih sistemov, Univerza v Mariboru, Fakulteta za strojništvo.